SCIENTIFIC REPORTS

OPEN

SUBJECT AREAS:
CHARACTERIZATION AND ANALYTICAL TECHNIQUES
POLYMERS
BIOINSPIRED MATERIALS
TISSUE ENGINEERING

Received
31 March 2014

Accepted
28 July 2014

Published
19 September 2014

Correspondence and requests for materials should be addressed to L.M. (l.moroni@maastrichtuniversity.nl) or F.F.R.D. (f.damanik@utwente.nl)

Towards an in vitro model mimicking the foreign body response: tailoring the surface properties of biomaterials to modulate extracellular matrix

Febriyani F. R. Damanik[1], Tonia C. Rothuizen[2], Clemens van Blitterswijk[1,3], Joris I. Rotmans[2] & Lorenzo Moroni[1,3]

[1]University of Twente, Drienerlolaan 5, Zuidhorst 145, 7522 NB Enschede, the Netherlands, [2]Department of Nephrology, Leiden University Medical Center, Albinusdreef 2, 2333ZA Leiden, The Netherlands, [3]Maastricht University, MERLN Institute for Technology Inspired Regenerative Medicine, Complex Tissue Regeneration, PO Box 616, 6200 MD Maastricht, The Netherlands.

Despite various studies to minimize host reaction following a biomaterial implantation, an appealing strategy in regenerative medicine is to actively use such an immune response to trigger and control tissue regeneration. We have developed an *in vitro* model to modulate the host response by tuning biomaterials' surface properties through surface modifications techniques as a new strategy for tissue regeneration applications. Results showed tunable surface topography, roughness, wettability, and chemistry by varying treatment type and exposure, allowing for the first time to correlate the effect of these surface properties on cell attachment, morphology, strength and proliferation, as well as proinflammatory (IL-1β, IL-6) and antiflammatory cytokines (TGF-β1, IL-10) secreted in medium, and protein expression of collagen and elastin. Surface microstructuring, derived from chloroform partial etching, increased surface roughness and oxygen content. This resulted in enhanced cell adhesion, strength and proliferation as well as a balance of soluble factors for optimum collagen and elastin synthesis for tissue regeneration. By linking surface parameters to cell activity, we could determine the fate of the regenerated tissue to create successful soft tissue-engineered replacement.

A foreign body reaction developing a fibrocellular capsule composed of (myo)fibroblast, macrophages, neutrophils, and foreign body giant cells is a result of an inflammatory response upon implantation of a biomaterial device[1]. Various studies in the field of biomedical engineering aim to reduce this cascade of host reaction, which is generally accepted as improvement of the implant biocompatibility[2,3]. Despite the need to reduce the host reaction to avoid extensive chronic inflammation and scar tissue, modulating the host response by designing materials with instructive properties could be advantageous for tissue regeneration strategies[4,5]. At present, researchers have introduced the concept of *in situ* tissue regeneration where the host response is used as an indirect way to attract specific host cells for tissue repair[6]. Similarly, *in situ* bioreactor strategies make use of the host environment and surrounding tissue to provide cells for tissue regeneration[7]. Surface properties of biocompatible materials are a critical factor in modulating the host response[1,8]. Initial cell and material interactions can be tailored by the chemical composition, hydrophilicity, surface roughness and topography of the implanted biomaterial[9]. Previous research have reported surface solvent etching to increase cell attachment on biomaterials[10]. Gas plasma techniques have also been extensively studied for their effect on biomaterial surfaces and cell attachment[11]. Although numerous studies aim at surface modification of implants to reduce the host response[2,12], tuning biomaterials surface properties to promote a suitable host response could be an appealing strategy to improve *in situ* tissue regeneration through an *in vivo* bioreactor approach. Furthermore, though various *in vitro* foreign body response (FBR) models have been proposed to study cell-cell signaling, correlation between cell activity followed by secretion of extracellular matrix (ECM) components with material properties is lacking[13–15]. Here, we propose a new strategy to modulate the host response for tissue regeneration applications. We present an *in vitro* co-culture model where tailoring surface properties results in deciphering the effect of surface wettability, topography, roughness and chemistry on cellular behavior with respect to cell adhesion and strength, proliferation, cytokine secretion, and expression of two main soft tissue extracellular matrix component, namely collagen and elastin.

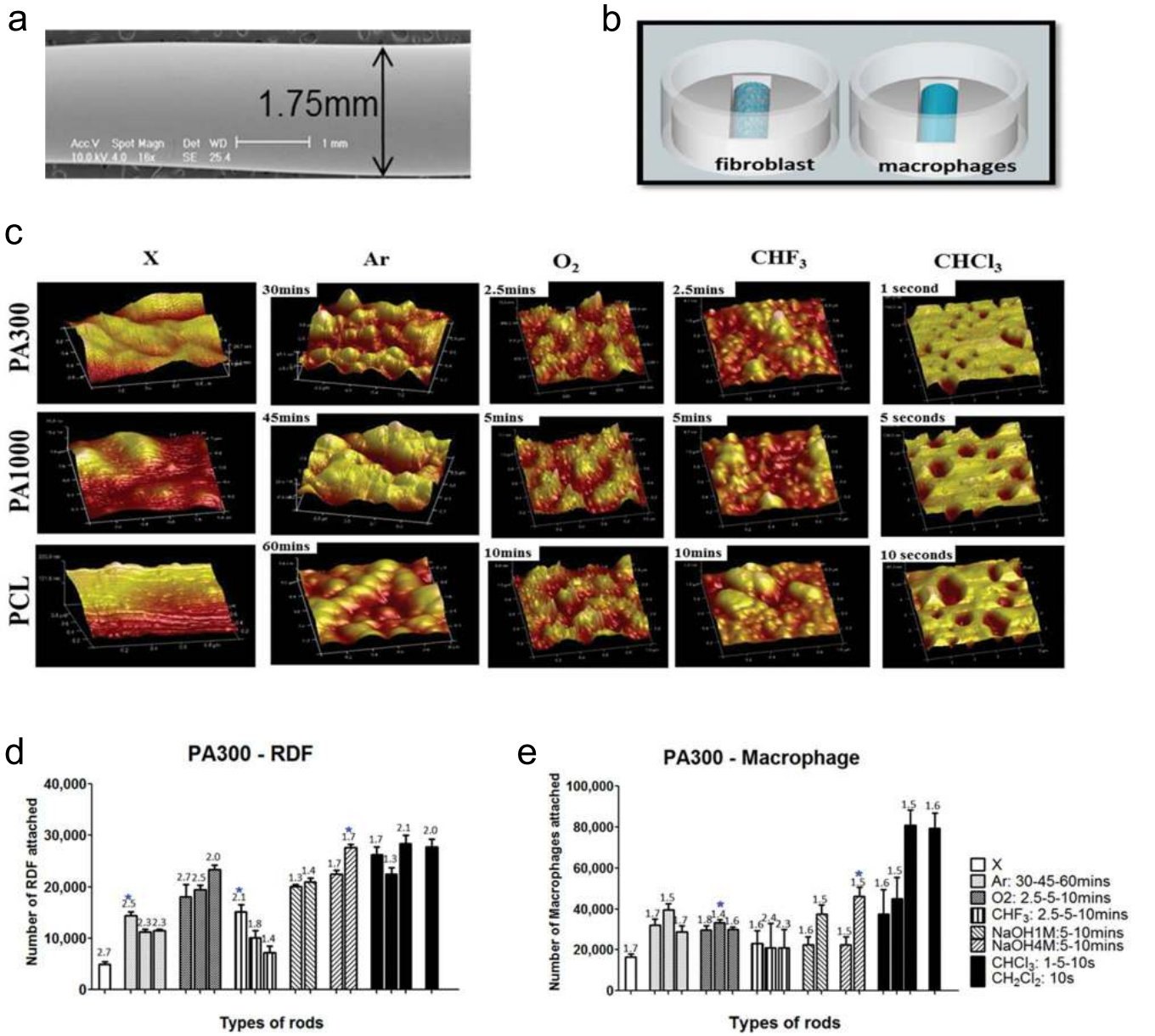

Figure 1 | Pre-selection of surface treatments. (a) SEM analysis of fabricated fiber (scale bar: 1 mm). (b) Scheme of mono-culture cell seeding on agarose mould. (c) 3D AFM images of PA300, PA1000 and PCL before and after different surface treatments and exposure time (scan size of 1 μm 2, with exception to $CHCl_3$ at 25 μm 2). DNA assay analysis of rat dermal fibroblasts (d) and macrophages (e) on PA300 at attachment. Unmodified (X) rods were subjected to either argon plasma treatment for 30, 45, and 60 minutes (Ar30–45–60, bars from left to right), oxygen or trifluoromethane plasma treatment for 2.5, 5, 10 minutes (O 2 2.5–5–10, CHF 3 2.5–5–10, bars from left to right). Other rods were treated with wet etching using either sodium hydroxide at 1 M or 4 M concentration for 5 and 10 minutes (NaOH1M:5–10, NaOH4M:5–10, bars from left to right), chloroform or dichloromethane for 1, 5 and 10 seconds ($CHCl_3$: 1–5–10 s, CH_2Cl_2–10 s, bars from left to right). The fold increase in cell number at day 3 can be seen above individual bars. RDF attachment was statistically increased in all treatments except for CHF 3 5–10 samples. Macrophage attachment increased significantly after Ar, O_2 and $CHCl_3$ treatments. Data are shown as mean ± s.d. (n = 3). Star (*, $P < 0.05$) indicates the best parameter for each treatment type.

Results

Scaffold fabrication from different polymeric composition. To facilitate our study of host response on biomaterials, we used a polymeric rod model, which was previously shown to be promising for vascular applications[16]. Polycaprolactone (PCL) and two co-polymer types of poly(ethylene oxide terephthalate)/poly(butylene terephtalate) (PEOT/PBT) - 300PEOT45PBT45 (PA300) and 1000-PEOT70PBT30 (PA1000) - were used to fabricate these polymeric rods, due to their satisfactory *in vitro* and *in vivo* biocompatibility, and easy tunable mechanical and physical properties by varying the PEOT/PBT ratio and the length of the PEO segments[17–19]. Ultra smooth fibers of 1.75 ± 0.05 mm diameter were extruded and characterized by scanning electron microscopy (SEM) and atomic force microscopy (AFM) (Fig. 1a; Supplementary Fig. S1,2). The surface roughness (Rq) of the fibers was as low as 5.2 ± 1.2 nm for PA300 and PA1000, and 8.3 ± 4 nm for PCL.

Surface modification of unmodified scaffolds. Smooth fibers were then treated with gas plasma or solvent etching to create different surface properties. Different gas plasma treatments were tested: argon (Ar) as an inert gas, oxygen (O_2) as an active gas, and trifluoromethane (CHF_3) providing hydrophobic surfaces in contrast to the

more hydrophilic argon and oxygen treatment[20–22]. Solvent etching was done with inorganic sodium hydroxide (NaOH) allowing alkaline hydrolysis and two organic compounds, chloroform ($CHCl_3$) and dichloromethane (CH_2Cl_2), providing physical etching[10,23]. AFM and SEM (Fig. 1c; Supplementary Fig. S1,2) analysis showed different topographical changes from the polymer types after treatment, and clear differences in surface structure at different exposure time, concentration, gas, and chemical used. By controlling the surface treatment parameters, we were able to vary surface roughness from 5.2 ± 1.2 nm for unmodified rods to 225 ± 25.1 nm as seen in $CHCl_3$ treated rods. By qualitatively comparing different polymer types after Ar treatment, we examined island-like structure on PA300, chain-like structure on PA1000 and random topography on PCL. O_2 treated rods produced peaks on island-like structure on PA300, and similar peak chain-like structure on PA1000, while CHF_3 resulted in grooves. Alkaline hydrolysis of NaOH induced topographical changes on PA1000 and PCL, but not on PA300. $CHCl_3$ and CH_2Cl_2 on the other hand provided small porous structures of 0.5–2.5 μm in diameter, surrounded by large porous structure up to 20 μm.

Mono-culture studies for cell attachment and proliferation. As fibroblasts and macrophages are among the key cells activated during the initial phases of the host response, we examined 17 different surface modifications in three polymer types, resulting in 54 experimental conditions, by culturing fibroblasts and macrophages separately to examine cell adhesion and proliferation (Fig. 1b,d,e; Supplementary Fig. S3–5). Results showed an increase in cell adhesion in all surface modified structures, with PA300 showing the most significant increase in comparison to the other polymer types. The best parameters of Ar, O_2, CHF_3, NaOH and $CHCl_3$ providing high cell adhesion and proliferation were chosen and compared to unmodified (X) to correlate surface properties to cell response.

Material characterization of surface hydrophillicity, roughness, chemistry and protein absorption. We further characterized the pre-selected rods to determine the surface roughness for cell and protein attachment, and contact angle measurement to determine wettability of the surface after treatment (Fig. 2a,b). Compared to unmodified rods, gas plasma treatments resulted in a 3-fold increase in surface roughness. Exposure time was modulated to maintain the surface roughness increase independent from the gas source used. $CHCl_3$ resulted in a 35-fold increase while NaOH lead to no increase in surface roughness. Hydrophillic surfaces (40°–70°) were created by Ar, O_2 and NaOH, while hydrophobic surfaces (80°–110°) by X, CHF_3 and $CHCl_3$. X-ray Photon Spectroscopy (Fig. 2c) showed doubling of oxygen content with Ar, O_2, NaOH, and $CHCl_3$ treatments. In contrast, CHF_3 treatment removed significant amounts of oxygen and carbon, and introduced C-F bonds instead. This justifies the high contact angle seen in CHF3 treated rods and the decrease in contact angle of Ar and O_2 treated rods despite having similar surface roughness as CHF_3. Protein absorption ability (Fig. 2d) of the different surfaces reflected the results on the available surface area (Supplementary Fig. S6) and wettability. Remnants of sodium (Na1s) and chloride (Cl2p) can be neglected due to their low amount.

Effect of cell adhesion on surface modified materials with conditioned medium. To further dissect the relation between macrophages and fibroblasts during fiber capsule formation, *in vitro* studies using a conditioned medium model were performed, where 50% of rat dermal fibroblasts (RDFs) and macrophage culture media were mixed and studied at day 1, 4 and 7 (Fig. 3a). As similarly seen in mono-culture studies, RDFs attachment and proliferation significantly increased upon different surface treatments, with $CHCl_3$ treatment having the best cell adhesion and proliferation in comparison to all the other treatments (Fig. 3b). Macrophage attachment and proliferation did not significantly increase, apart for $CHCl_3$ treated rods. In general, conditioned medium provided higher proliferation in comparison to refresh medium in both cultures. Cell distribution (Fig. 3c,d) reflected cell proliferation results, with more cell homogeneous attachment in treated rods. Hydrophillic Ar and O_2 treated rods created a homologous tissue layer around the rods. In comparison, CHF_3 and NaOH etched rods created a less homogeneous cell distribution.

Surface characteristics versus soluble factors secretion. To steer the host response towards functional tissue regeneration during fiber capsule formation through the design of biomaterial surfaces, it is important to identify what kind of cytokines and growth factor are secreted and how they interact with each other. Here, we tested TGF-β1 and IL-10 for M2 wound healing phenotype, and IL-1β and IL-6 for M1 inflammation type[32]. Active TGF-β1 was measured both in RDFs and macrophage cultures (Fig. 4a). At day 1, Ar and O_2 treated rods, with 3-fold higher surface roughness, 2-fold higher oxygen content and 20°–30° lower contact angle compared to unmodified rods, provided a 2-fold upregulation of TGF-β1. The difference in hydrophillicity of Ar and O_2 of 10° seemed to have no effect on the upregulation of TGF-β1. CHF_3 treated rods, with similar roughness of Ar and O_2, but 20-fold lower oxygen content and 40°–50° higher contact angle, resulted in a decrease of TGF-β1 compared to unmodified rods. Importance in surface chemistry was further corroborated by NaOH etched rods, with 1.5-fold increase in oxygen content and 50° lower contact angle, resulted in an increase of TGF-β1 compared to unmodified rods. A further increase in surface roughness to 35 folds as seen in $CHCl_3$ treated rods, and about 2-fold increase in oxygen content, provided about 2-fold upregulation of TGF-β1 compared to unmodified rods. In macrophage cultures, significant increase in TGF-β1 production was measured in CHF_3 and $CHCl_3$ treated rods, no significant upregulation in Ar and O_2, and downregulation in NaOH treated rods compared to unmodified ones. An upregulation trend of TGF-β1 in RDFs (Supplementary Fig. S7) at day 4 was seen after addition of conditioned medium from macrophages. This was slightly the opposite for macrophage culture, where after exposure to RDF's conditioned medium, TGF-β1 expression was reduced. For RDFs at day 7, TGF-β1 decreased for all treatments except for $CHCl_3$. IL-10 (Fig. 4b) was expressed more in hydrophillic surfaces (Ar, O_2 and NaOH treated rods). In our studies, we also observed downregulation of IL-1β and IL-6 in hydrophilic surfaces and upregulation of these cytokines in hydrophobic surfaces (CHF_3 and $CHCl_3$). For all treated rods, upregulation of IL-10 was seen at day 4 after exposure to RDF's conditioned medium incubated for 24 hours. After further exposure, IL-10 expression decreased at day 7, with exception of $CHCl_3$ treated rods, similar to TGF-β1 expression. Inflammatory cytokines IL-1β and IL-6 expression displayed opposite trends than IL-10, as they were upregulated in hydrophobic surfaces (X, CHF_3 and $CHCl_3$) and downregulated in hydrophilic surfaces. Downregulation of both inflammatory cytokines IL-1β and IL-6 was seen at day 4 and day 7 with conditioned medium culture being more downregulated. By evaluating total amount of soluble factors produced (Supplementary Fig. S8), $CHCl_3$ treated rods produced the highest amount of TGF-β1, IL-1β, IL-6 and IL-10, creating a more significant and dynamic effect on tissue capsule formation.

Immunostaining of material's surface to macrophage topography link. From a morphological perspective, variations in surface wettability, chemistry, and topography also influenced cell shape. An unmodified surface of PA300 (Fig. 4c) induced extension of macrophage filopodia. Further cytoplasmic extensions, which are used for locomotion as the macrophages seek out to engulf foreign particle, were seen in nanoscale modification of Ar, O_2, and CHF_3. Microscale topography change in $CHCl_3$ drove more filopodia compared to unmodified rods, though not to the extent of

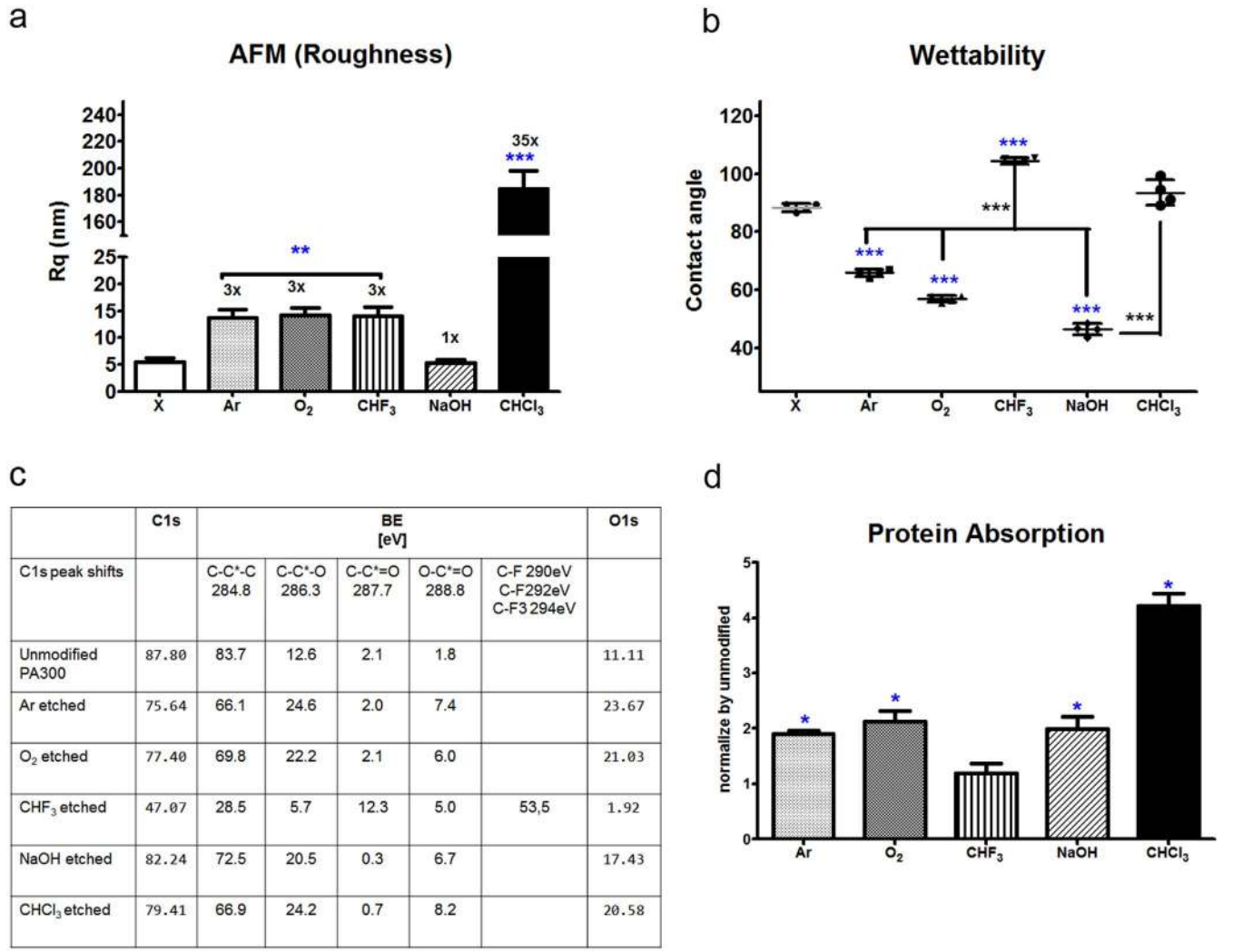

c

	C1s	BE [eV]					O1s
C1s peak shifts		C-C*-C 284.8	C-C*-O 286.3	C-C*=O 287.7	O-C*=O 288.8	C-F 290eV C-F292eV C-F3 294eV	
Unmodified PA300	87.80	83.7	12.6	2.1	1.8		11.11
Ar etched	75.64	66.1	24.6	2.0	7.4		23.67
O_2 etched	77.40	69.8	22.2	2.1	6.0		21.03
CHF_3 etched	47.07	28.5	5.7	12.3	5.0	53,5	1.92
NaOH etched	82.24	72.5	20.5	0.3	6.7		17.43
$CHCl_3$ etched	79.41	66.9	24.2	0.7	8.2		20.58

Figure 2 | Material characterization of pre-selected treatments. (a) AFM roughness quantification (Rq at scan size 1 μm). The number of folds each treated rod increase in roughness is shown above its bar. (b) Hydrophilic treatments (70–40°) consisted of Ar, O_2 and NaOH, while hydrophobic treatments (85–110°) consisted of CHF 3 and $CHCl_3$) (n = 4). (c) XPS measurement on unmodified versus pre-selected modified rods. Groups of 2-fold increase (Ar, O_2, NaOH and $CHCl_3$) and 5-fold decrease (CHF 3) in oxygen content can be seen. (d) Protein absorption assay on unmodified versus pre-selected modified rods. Protein absorption in modified rods was normalized by the protein absorption in unmodified rods, thus showing fold differences between the different treatments. All data are shown as mean ± s.d. (n = 3), if not stated otherwise. Blue stars (*P < 0.05, ** P < 0.01, *** P < 0.001) indicate statistically significant values in comparison to unmodified (X), black stars compares each treatments to one another.

nanoscale modifications. Further activation was seen both in microscale and nanoscale topography, as shown by the vacuoles presented on the surface of the macrophage. Smooth hydrophillic surface (NaOH treatment) provided less branching, but more spreading. Similar morphology was seen in phalloidin and dapi staining, with additional information on the fusion of the macrophages to form giant cells (Supplementary Fig. S9). All treatment showed similar fusion.

Immunostaining of material's surface to fibroblast topography link. We analyzed fibroblast morphology on the different surface treated biomaterials (Fig. 5a,b; Supplementary Fig. S10,11,). Homogenous spread morphology was observed on surfaces with high oxygen content and increased surface roughness, as seen in both Ar and O_2 sheets. Two types of population of cells were found in X, CHF_3, NaOH and $CHCl_3$. In X, NaOH, and CHF_3, the first population displayed smaller and less spread cells, with little or no vinculin staining showing focal adhesion sites. The second population showed polygonal morphology, with more define vinculin sites connected to the enhance actin stress fibers. For $CHCl_3$, despite having some smaller cells, both cell populations provided a spread morphology, yet with different vinculin expression (8.7 ± 0.7 μm^2, 16.7 ± 1.52 μm^2). Smaller condensed strokes of vinculin localization were found on large porous structure, whereas vinculin expression on smaller pores produced more elongated sites. Quantification of vinculin on cell population expressing vinculin dots (Supplementary Fig. S10) provided values of average area, perimeter, circularity, length, width and the aspect ratio of the vinculin sites to deduce cell adhesion strength. When comparing X and $CHCl_3$ for average area, length, aspect ratio and circularity, smoother surfaces provided a larger average area, length and aspect ratio of vinculin sites, while rougher surfaces provided higher circularity. From a comparison between different surface plasma treatments having the same roughness, but different surface wettability, it could be also concluded that the increase in focal adhesion area is proportional to the substrate contact angle. In case of width, CHF_3 provided the widest value compared to all the other treatments. Moreover, O_2 showed to have the longest length and aspect ratio. The total amount of vinculin staining was then normalized by the number of cells of both populations (Figure 5c). Vinculin area per

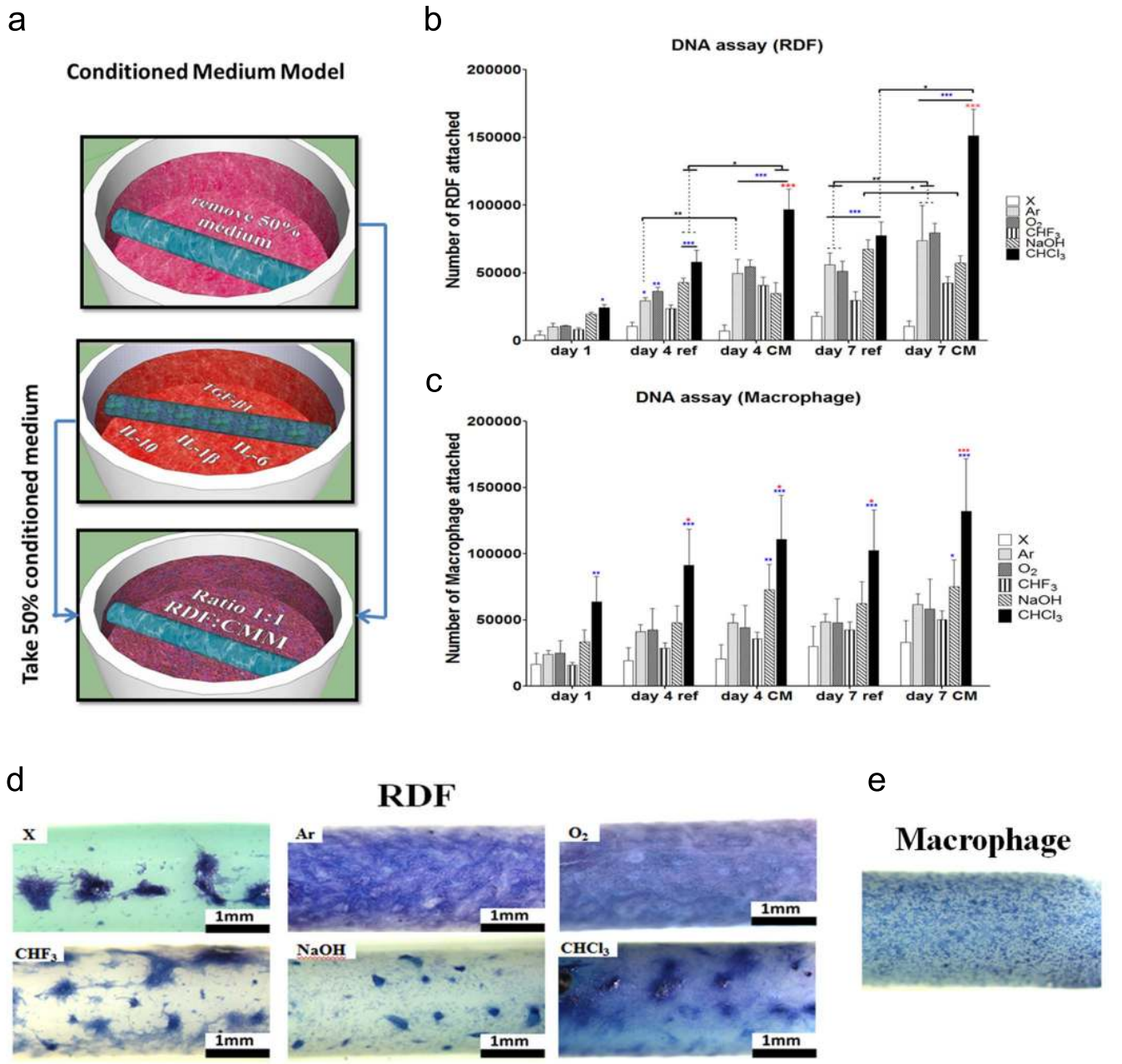

Figure 3 | Conditioned medium co-culture in vitro studies on unmodified versus modified rods. (a) Conditioned medium co-culture scheme. DNA assay on RDFs (b) and macrophage (c) seeded rods, at day 1, 4 and 7 and with (CM) or without (ref) conditioned medium (X-axis). Different surface treatment are represented by different bar patterns. RDFs attachment was statistically increased ($P < 0.05$) in all treatments except for CHF35-10 samples. Data are shown as mean ± s.d. (n = 3). Blue stars (*$P < 0.05$, ** $P < 0.01$, *** $P < 0.001$) indicate statistical significances in comparison to unmodified, red stars indicate the best parameter from all the treatment types, while black stars evaluate statistical differences between the different culture conditions. Illustration of cell distribution at day 4 of RDFs (d) and macrophages (e) via methylene blue staining (scale bar: 1 mm). RDFs illustrated above showed different distribution of cells dependent on the treatment, while in all treatments distribution of macrophages were alike.

cell displayed a significantly higher difference between X and $CHCl_3$. In measuring the amount of vinculin dots per cell, however, $CHCl_3$ supported a significantly higher amount than X and NaOH with similar surface chemistry (oxygen content), showing a distinct effect of surface roughness (Supplementary Fig. S10).

Extracellular matrix composition analysis for the ideal tissue capsule. Collagen and elastin production (Fig. 5d,e; Supplementary Fig. S11) are crucial factors to create functional connective tissues, such as dermis, cartilage and vessels. Our chosen surface modification techniques have statistically significantly triggered an increase in both total collagen and elastin production in day 4 and day 7 cultures of RDFs. In comparison to standard culture medium, conditioned medium created a statistically significant increase of total elastin at day 7 and per cell at day 4, and both total and per cell collagen production at day 4 and 7. The importance of surface chemistry was further seen when comparing O_2 and CHF_3 treatments in refresh medium cultures, where collagen and elastin secretion was higher in oxygen content despite similar surface roughness. $CHCl_3$ treatment provided the highest increase of total collagen and collagen/cell secretion, as well as total elastin secretion compared to all the other treatment types and unmodified rods.

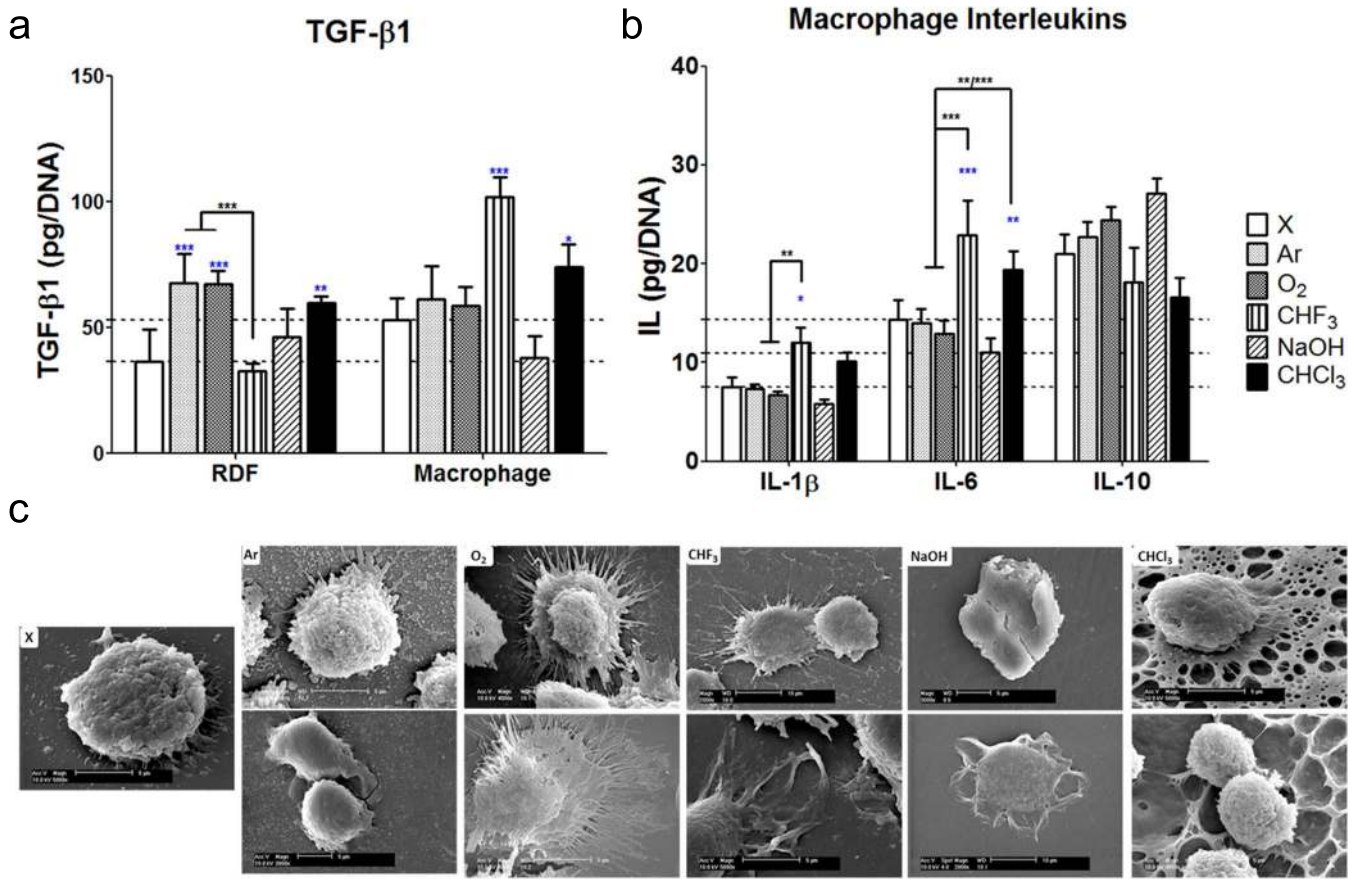

Figure 4 | Cytokine analysis on conditioned medium co-culture in vitro studies. (a) TGF-β1 secretion in RDFs and macrophages at day 1. (b) Interleukin (IL-1β, IL-6 and IL-10) expression in macrophages in mono (ref) or conditioned medium co-cultures (CM) at day 1. Normalized per DNA represent amount secreted for 100,000 cells. Each horizontal tick is in reference to TGF-β1 RDFs and macrophages (a), and IL-1β, IL-6 and IL-10 macrophage (b) value of unmodified rods. Data are shown as mean ± s.d. (n = 3). Blue stars (*P < 0.05, ** P < 0.01, *** P < 0.001) indicate statistical significances in comparison to unmodified, and black stars evaluate statistical differences between the different treatments. (c) SEM images (scale bar: 5 and 10 μm) show different macrophage morphology on different surface treatments in mono-culture study. Filopodia of macrophages seeded on nano-scale modification of Ar, O_2, and CHF3 were more extended compared to $CHCl_3$ providing micro-scale modification on its surface, and NaOH providing no surface topography modification.

Discussion

Here, we have fabricated rods of different surface properties to unravel specific parameters on modulating host response. Different polymer composition could affect the degree of surface modification as shown in AFM & SEM analysis. Higher amount of crystalline PBT in PA300, which is hydrolysis resistant, provided no change to topography upon NaOH treatment in contrast to polymer with low PBT. Surface properties, namely chemistry, topography and wettability, are interdependent parameters. Chemical -CF_2- groups are larger compared to -CH_2- groups, allowing fewer groups to be packed into a given area. This justifies the high contact angle seen in CHF_3 treated rods and the decrease in contact angle of Ar and O_2 treated rods despite having similar surface roughness as CHF_3. Similarly, NaOH treated rods with high oxygen content and similar surface roughness to unmodified rods, had lower contact angle. We could extrapolate that a similar wettability was seen for $CHCl_3$ treated rods in comparison to unmodified rods despite its high oxygen content, possibly due to the high surface roughness and the interaction of water molecules with its porous structure at the interface[24,25]. By taking advantages of these many parameters and their effects, we can envision to create tailored surface properties suitable for a specific tissue engineered application.

Combination of physico-chemical properties are crucial for proper tissue regeneration. Rougher, hydrophilic surfaces with high oxygen content observed in Ar and O_2, displayed homogenous spreading of cells with enhanced stress fibers and focal adhesion sites. In X, CHF_3 and NaOH rods, cells have a tendency to migrate and prefer to attach to each other than to the surface of the biomaterial. As similarly shown by de Rocha-Azevedo et. al.[26], this could be due to the lack of carbon and oxygen content but high content of fluoride in CHF_3 treated rods, or lack of surface roughness in X and NaOH etched rods. This then could explain the lack of stress fibers and vinculin expression on the first population of cells. As cells start to migrate to one another, paracrine signaling from other cells are transmitted to provide additional signal transduction. Paracrine factors can either bind to their respective cellular receptor directly initiating the associated specific pathways, such as TGF-β1 signaling pathway, or through intracellular Calcium level resulting in integrin activation through talin. Talin presence is required for vinculin recruitment which then starts actin polymerization, resulting in actin stress fibers on the second cell population[27]. High surface roughness and correspondent surface area availability provided after $CHCl_3$ treatment allowed more cells to attach and proliferate, as well as total vinculin expression per cell, suggesting a stronger attachment of cells on $CHCl_3$ treated surfaces. Micro-scale topography changes, creating homogenous pores on the surface, are also a crucial factor[28]. Vinculin staining displayed different expression of focal adhesion sites on small and large pores of $CHCl_3$, suggesting different cell behavior. Lee et al.[29] showed that fibroblasts cultured on polycarbonate membranes with different micropore sizes (0.2 and 8.0 μm), displayed a

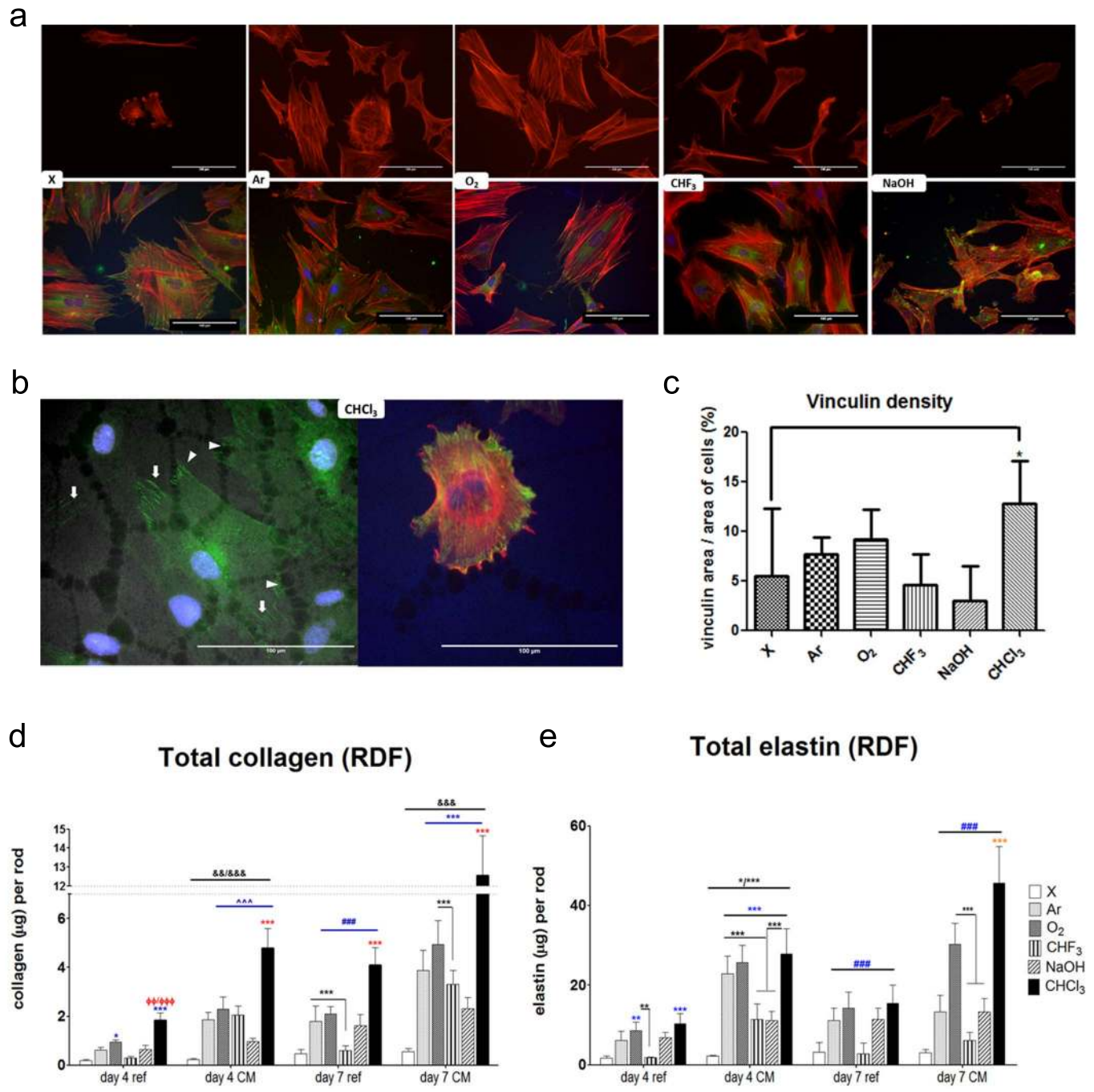

Figure 5 | **Focal adhesion immunostaining and total collagen and elastin synthesis.** (a) Immunostaining images (scale bar: 100 µm) of RDFs show vinculin (green), phalloidin (red) and dapi (blue) on different surface modification type. The upper panel shows staining for phalloidin only to exhibit the first population of RDFs morphology on X, CHF 3 and NaOH, where cells were poorly spread. The lower panel shows that the second population of RDFs morphology on X, CHF 3 and NaOH, where cells were more spread, exhibited vinculin sites and organized actin cytoskeleton. Ar and O_2 provided a homogenous spread of cells, enhanced actin stress fibers and vinculin expression throughout the polymer. (b) $CHCl_3$ displayed a homogenous population of cells with enhanced actin filaments expression, but different vinculin density. Vinculin sites found in larger pores (5–20 µm) shown by the arrow heads expressed dense circular vinculin sites, while smaller pores (0.5–2.5 µm) displayed by the arrows expressed elongated vinculin staining. (c) Quantification of vinculin density per treatment. Statistics were done by One-way ANOVA with a post Tukey test (n = 8). (d) Quantification of collagen secreted per different rod showed statistically significant increase in production after surface modification for day 4 conditioned medium (CM), day 7 refresh medium (ref) and CM (^ indicating exception to NaOH, # to CHF 3). CM cultures triggered a significant increase in comparison to refresh medium, (& indicating exception to CHF 3 and O_2). $CHCl_3$ secreted the highest collagen amount in comparison to all treatments (red star, or Φ indicating exception to O_2). (e) A statistically significant increase of elastin secretion was seen on treated rods for day 4 conditioned medium (CM), day 7 refresh medium (ref) and CM (# indicating exception to CHF 3). CM cultures triggered a significant increase in comparison to refresh medium on day 4. At day 7 CM, $CHCl_3$ provided the best secretion of elastin in comparison to all other surface modification. Data are shown as mean ± s.d. (n = 6). Blue symbols (*$P < 0.05$, ** $P < 0.01$, *** $P < 0.001$) indicate statistical significances in comparison to unmodified, red symbols indicate the best parameter from all the treatment types, and black symbols evaluate statistical differences between the different treatments.

decreased cell adhesion and proliferation with increasing pore size. Furthermore, an increase in pore size improved cell differentiation as resulting from a higher osteocalcin expression and ALP specific activity. Hence, extrapolating these findings to our study one could suggest that a combination of different pore size with appropriate surface chemistry may contribute to the combination of optimal cell adhesion and proliferation from the small pores interaction and secretion of beneficial proteins from the large pores of $CHCl_3$ cell-material interaction. Furthermore, the high oxygen content microporous structure of $CHCl_3$ allowed cells to cover the surface of the rod and provided a potential buildup of layers of cells through support of cell accumulation in its large micropores. Moreover, as $CHCl_3$ treated rod absorbed the highest amount of proteins, a higher trigger of signal transduction compared to all other treatments could be suggested as seen in Yang et. al[27]. Strong interconnectivity between different surface parameters, may provide some challenges in decoupling their effect on bioactivity. However, by sensitively tuning different parameter separately we could come closer to unraveling the link.

During host reaction upon biomaterial implantation, the healing response is triggered by the action of macrophages and is identified by the proliferation of fibroblasts, synthesis of collagen and proteoglycans, and angiogenesis[1]. To mimic such a host response, we use an *in vitro* co-culture conditioned medium model using macrophages and fibroblast. Macrophage polarization represents a continuum where it provides a balance between the pro- and anti-inflammatory responses by alternating from classically (M1) or alternatively (M2) activated macrophages[30,31]. Critical to the actions of these divergent or polarized macrophage clusters, is the regulated release of inflammatory mediators. M1 phenotype macrophages display a more pro-inflammatory response driven by interleukins (IL) such as IL-1β and IL-6, while the alternate M2 phenotype suppress immune and anti-inflammatory processes in favor of extracellular matrix formation, angiogenesis, and tissue repair driven by IL-10 and TGF-β1[30,32]. The balance between the different mediators during an implantation will determine the outcome of the host response and viability of the functional tissue capsule. Additional cytokines and growth factors produced by the opposed cell culture would provide reason why cultures with conditioned medium have a higher proliferation in comparison to refresh medium in both cell types. Increase in down-regulation of both inflammatory cytokines IL-1β and IL-6 at later stage of host response, were observed in conditioned medium culture. This implies a reduced inflammatory response and balancing of M1 and M2 phenotype cytokine secretion, settling a step to determine the outcome of expected tissue capsule formation. Latent TGF-β1 is normally activated to influence wound healing from the initial cell-material interaction to the final phase of matrix deposition and remodeling[33]. Through our observation of TGF-β1 regulation from modulating surface parameters separately, one could suggest that oxygen content is a more dominant factor for TGF-β1 regulation than surface roughness and wettability for fibroblasts. Other properties such as the high fluoride content present in CHF_3 treated rods could be one of the factors behind the observed increase in TGF-β1 expression compared to Ar and O_2 treatments, while the increase of wettability in NaOH treated rods could be responsible for the observed TGF-β1 downregulation, comparable to other studies[34–36]. $CHCl_3$ creation of a porous structures could also induce activation of TGF-β1 upregulation from its topography[37–39] and Barth et al., showed macrophages cultured on rougher surfaces tend to resemble the activity of an M2-like phenotype[38]. We hypothesize the above environmental stress of hydrophobicity, high fluoride content and surface roughness on the macrophage cell surface may lead to activation of TGF-β1[40,41]. In conditioned medium, upregulation in RDFs could be caused by interaction of different pro-inflammatory cytokines produced by the activated macrophage such as IL-1β and TNF-α; while possible anti-inflammatory cytokines secreted by RDFs, such as IL-10, induced a downregulation of TGF-β1 in macrophages[42,43]. Our results are in line with previous observations where hydrophilic surfaces resulted in downregulation of TNF-α, IL-1β and IL-6 and upregulation of IL-10[44]. Hydrophobic surfaces was found to upregulate IL-1β and IL-6. This may correlates with the hypothesis of Seong et al., that hydrophobic surfaces provide a hostile surface for initial protein attachment similar to damage associated molecular pattern that initiates innate immune responses[45–47]. From these data showing different cytokine production correlated to surface wettability, chemistry, and roughness with and without conditioned medium of different cell types, it is crucial to further study the cross-talk between fibroblasts and macrophages with different co-culture models in an effort to unravel their complex interaction in the foreign body response *in vivo*.

Cell morphology is regulated by the internal organization of the cytoskeletal networks by initial cell-material and cell-cell interaction and structural features are known to influence signal transduction and the integration of intracellular signaling[48]. Immunostaining of macrophage cytoskeleton provided some evidence of fusion. Further analysis to quantify the ratio of the different stages of fusion of the different treatments and how this correlates with the different mediators secreted would be beneficial. However, a different type of co-culture model should be used to allow direct cell-to-cell contact to analyze fusion and formation of foreign body giant cells.

Collagen is the main ECM protein that is essential for the mechanical characteristics of (tissue engineered) blood vessels[49]. For vascular grafts, elastin is an important structural and regulatory matrix protein and plays a dominant role by conferring elasticity to the vessel wall[50]. Fibroblast are capable of synthesizing tropoelastin monomer, which is cross-linked and structured into elastin forming concentric rings of elastic lamellae around the medial layer of vessels[51]. Therefore, enhancing fibroblast elastin production could be a crucial link of successfully creating tissue engineering blood vessel[52]. Yet, no studies have found and targeted elastin synthesis in a fibrocellular capsule. The trigger for elastin synthesis, however, is not completely understood, but includes exposure to mechanical stress and presence of growth factor such as TGF-β1[53]. In this study, techniques to modified the surface of biomaterials have statistically significantly triggered an increase in both total collagen and elastin production, conceivably due to the observed enhanced production of cytokines, such as TGF-β1 as a key enhancer of collagen production and providing support for elastin secretion[50,54,55]. Conditioned medium created a statistically significant increase of both elastin and collagen production in comparison to standard culture medium. This could be correlated to the additional soluble factors such as TGF-β1 and IL-10 produced by macrophages in conditioned medium. Additionally, cytokines analysis shows correlation with collagen and elastin expression. IL-10, which was upregulated in hydrophilic surfaces is a major mediator of matrix remodeling and correlates with total amount of collagen and elastin expressed. In our study, upregulation of IL-1β associate with the downregulation of collagen and elastin production, comparable to previous studies[56,57]. On contrast, a few studies show that IL-6 could provide upregulation of collagen and elastin secretion[58,59]. It is the combination of these factors, among others, that signals a cell to produce more or less collagen and elastin. This balance of cytokines produced through surface topography and chemistry in $CHCl_3$ treatment provided the best condition collagen and elastin secretion compared to all the other treatment types and unmodified rods. We hypothesize, that collagen and elastin expression is correlated to surface roughness, wettability, and oxygen content. Additionally, the increase in secreted matrix elements like collagen and elastin could be due to either protein secretions at the cellular level or gene expression at the molecular level. Hence, studies to examine other mediators of collagen and elastin synthesis would be beneficial to further understand their involvement at cellular and genetic levels.

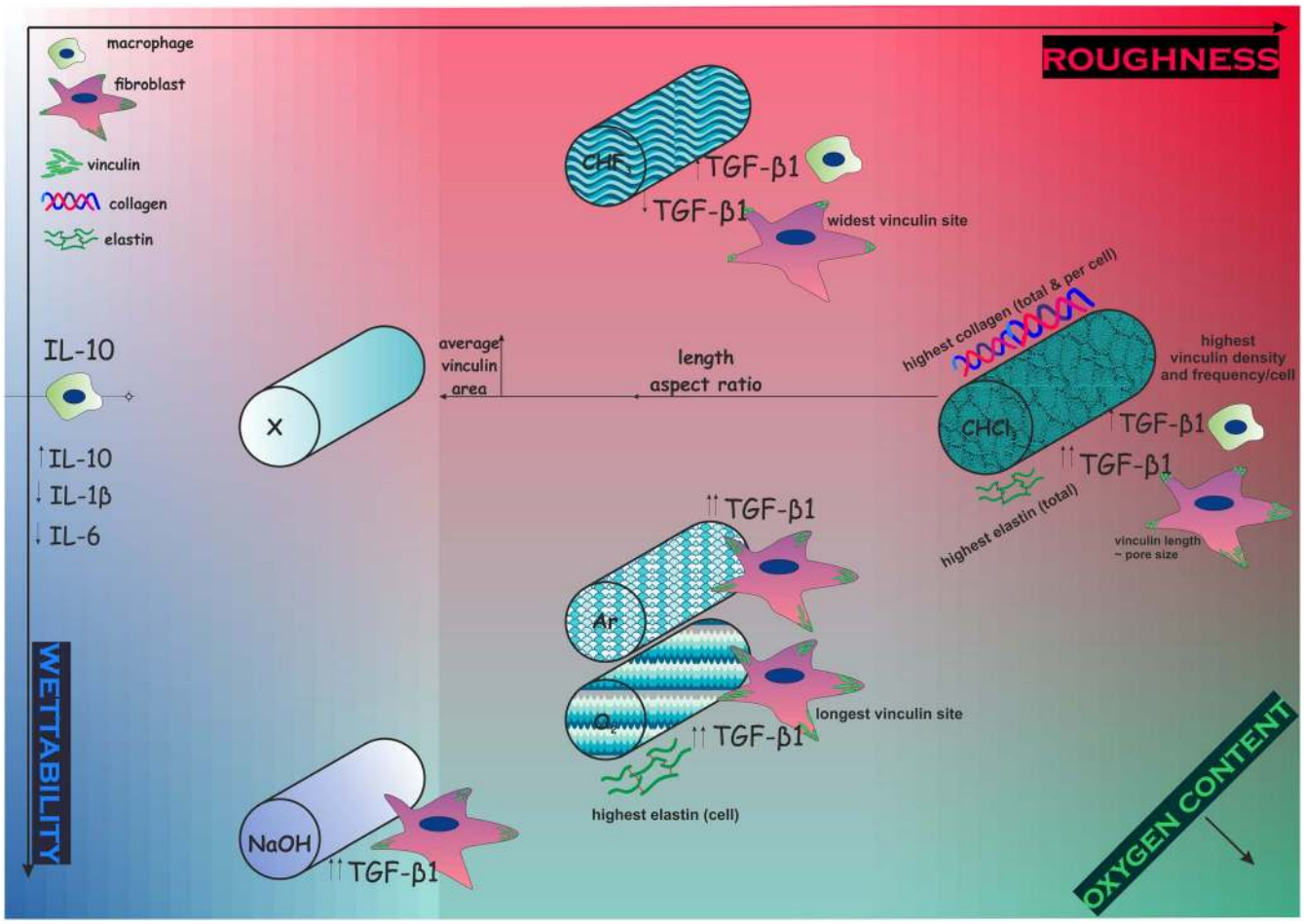

Figure 6 | Schematic correlation between surface properties and cell behavior from cytokine levels, extracellular matrix composition and focal adhesion properties. Colour background represent degree of roughness (red), wettability (blue) and oxygen content (green). Unmodified rods (X), were treated with five surface treatments (NaOH, CHF 3, Ar, O 2, and CHCl 3), to produce different surface topography, oxygen content, wettability and roughness. These properties are correlated with the different cell behaviour in regards to cytokine secretion, elastin and collagen production, and vinculin expression.

In summary and as seen in Fig. 6, we have shown different surface treatments resulted in a modulation of surface properties and furthermore, modulating its effect on cell behaviour of the main players in a host reaction through *in vitro* co-culture. All treatments provided an increase in cell attachment and proliferation, with the micro-porous structure of $CHCl_3$ providing the best cell adhesion and proliferation due to its the high surface roughness and high oxygen content. Furthermore, combination of different pore size, contributed to different cell adhesion strength, allowing the two cell population in $CHCl_3$ to mediate proliferation and secretion of essential proteins. Mediators of pro and anti-inflammatory response were regulated via surface roughness and resulting topography, wettability and chemistry at different levels. TGF-β1 regulation in RDFs was upregulated through oxygen content, while activation of TGF-β1 in macrophage was triggered from environmental stress of hydrophobicity, high fluoride content and surface roughness. Hydrophillic surfaces upregulated IL-10 expression, but downregulated IL-1β and IL-6, in contrast to hydrophobic surfaces that upregulated IL-1β and IL-6 expression. Most importantly, $CHCl_3$ treated rods provided the highest amount of TGF-β1, IL-1β, IL-6 and IL-10, with the ideal balance to deliver enhanced collagen and elastin secretion, which determines the fate of the tissue regeneration and functionality, and could possibly be the missing link to create successful soft tissue-engineered replacements.

Methods

Fabrication of polymeric scaffold: rods and sheets. PA300 and PA1000 (PolyVation B.V.) copolymers rods were manufactured with a Bioplotter device (Envisiontec GmbH), an XYZ plotter device as previously described by Moroni et. al[60]. Briefly, polymer granules were loaded to a stainless steel syringe and heated at 180°C. At 4–5 bars, the bioploter computer aided manufacturing software (CAM, PrimCAM) was used to plot the extrusion to achieve cylindrical fibers of 1.75 mm. PCL (Purasorb PC 12, Purac Biomaterials, The Netherlands) rods were fabricated via an Axon Mini extruder (BX-12, Axon AB Plastmaskiner), using a spinning pump (Mahr GmbH) at 12.2 rpm (0.6 cc/rev), 170°C and a pressure of 25 bar. 2D polymer substrates of PA300 were prepared for immunostaining studies. 2D PA300 disc of 500 μm thickness were made by a hot-embossed compression molding technique. Granules of PA300 were distributed inside circular punched molds of stainless steel and was placed between two silicon wafers functionalized with 1H,1H,2H,2H-perfluorodecyltrichorosilane (FDTS, Sigma-Aldrich). The wafer-mold-wafer stack was placed in the aperture of the temperature hydraulic press (Fortune Holland) at 180°C and 10 bar. After 5 minutes the system was cooled to 60°C and the pressure was released. The mold and wafer were manually separated to provide smooth PA300 discs.

Surface treatments – gas plasma & chemical etching. Ar plasma treatment was done with a Harrick Plasma Cleaner (PDC-002;. Harrick Plasma Ithaca) at 100 mTorr and High settings (740 V DC, 40 mA DC, 29.6 W) for 30, 45, and 60 minutes, respectively. O_2 and CHF_3 treatments were performed with a reactive ion etch system (Etch RIE Tetske, Nanolab, University Twente) at 100 mTorr and 30 W for 5, 10, and 15 minutes. NaOH etching was performed at 1 M and 4 M for 5, 10, and 15 minutes. Fibers etched with $CHCl_3$and CH_2Cl_3 were exposed for 1, 5 and 10 seconds. After inorganic and organic etching, fibers were rinsed once with MilliQ water and further sonicated two times for 15 minutes each.

Atomic force microscopy (AFM) - surface roughness and 3D images. Surface roughness analysis was performed through AFM using Tapping Mode (PicoScan Controller 2500, Molecular Imaging, USA) with a super sharp TESP cantilever: 42 N/m, 320 kHz, 2–5 nm ROC, No Coatings (Bruker AFM Probes.). The roughness measurements (Ra, Rq, and Rmax) were determined using the Scanning Probe Image Processor, SPIPTM, version 4.2.2.0 software. Roughness measurements were performed by 1, 25 and 100 μm^2 surface area. High quality images in three dimensions (3D) of the polymer's surface were recorded and repeated three times at randomly different surface locations to verify the reproducibility of the observed characteristics.

Contact angle and x-ray photon spectroscopy. Wettability measurements were done by static water contact angle measurements using the captive bubble method (OCA 15, DataPhysics Instruments GmbH). Water contact angle (~1 μL) was calculated using SCA20 software (DataPhysics Instruments GmbH). Subsequently, the rods were transferred to the XPS chamber. The XPS chamber (Omicron Nanotechnology GmbH) had a base pressure below 1×10^{-10} mbar. The measurements were done using a monochromatic Al Kα (XM 1000) X-ray source and an EA 125 electron energy analyzer. All spectra were acquired in the Constant Analyzer Energy (CAE) mode. XPS spectral lines are identified by the shell from which the electron was ejected (1s, 2s, 2p, etc.).

Cell culture and expansion. Neonatal rat dermal fibroblasts (RDF, R106-05n, Tebubio Cell Application, Inc.) were cultured with basic culture medium comprising α-MEM (Gibco), fetal bovine serum (10%, Lonza), L-glutamine (2 mM, Gibco) and penicillin (100 U/ml) and streptomycin (100 mg/ml, Gibco). RDFs were expanded at initial seeding density of 3000 cells/cm^2 in basic culture medium and refreshed every 2–3 days. Cells were harvested at 80–90% confluency before trypsinzation for cell seeding. A rat alveolar macrophage cell line NR8383 (ATCC) and maintained in basic culture medium with at 200,000 cells/ml. Subculturing was done by transfer of medium to another flask, and collection of cells by scraping with a Corning® cell scrapers (Sigma-Aldrich). All cell experiments were performed in a 5% CO_2 humid atmosphere at 37°C.

Mono-culture cell seeding of fibroblasts and macrophages. Modified and unmodified fibers (n = 3) were cut into 1 cm rods per sample and sterilized with 70% ethanol. Rods were pre-incubated for 4 hours in basic culture medium. Agarose molds (3% wt/v) were placed below the rods to prevent cell attachment to 48 well-plates and for optimum static cell seeding. A cell seeding density of 50,000 RDFs and 100,000 macrophages was seeded in a 500 μl volume. Samples were rinsed with phosphate buffered saline (PBS, Invitrogen Life Technologies) and collected at day 1 and day 3 for DNA assay, and imaging with methylene blue (MB) and scanning electron microscopy (SEM).

Conditioned medium co-culture study. Similar to monoculture study, fibers of 1 cm rods were sterilized with 70% ethanol, placed on top of agarose molds and pre-incubated for 4 hours in basic culture medium. A cell seeding density of 50,000 RDFs and 100,000 macrophages was seeded in a 250 μl volume. 24 hours after cell seeding, 50% of RDF and macrophage culture media were mixed and studied at day 1, 4 and 7, for DNA, ELISA, collagen and elastin assay, MB, immunostaining and SEM.

Cell proliferation assay. Total DNA was measured with the CyQuant Cell Proliferation Assay kit (Molecular Probes) to access cell adhesion and proliferation. Briefly, samples (n = 3) were washed gently with PBS and collected into a 500 μl eppendorf tube and frozen at −80°C. After freeze-thawing for three times, lysis buffer (250 μl, 1 : 20 Lysis buffer 20×) was added to the samples at room temperature (RT) for 1 hour, and an additional 1 hour with lysis buffer RNase. Subsequently, cell lysate and CyQuant GR dye (1×) were mixed 1 : 1 in a white 96-well plate and incubated in the dark for 15 minutes. Fluorescence was measured at an excitation and emission wavelengths of 480 and 520 nm, respectively, using a spectrophotometer (The VICTOR³ Multilabel Plate Reader Perkin Elmer Corporation).

Methylene blue staining, immunostaining and scanning electron microscopy. Chemicals were supplied by Sigma Aldrich, if not stated otherwise. Samples (n = 5) were washed with PBS and fixed with 4% paraformaldehyde for 30 minutes at RT. After rinsing with PBS, samples (n = 2) were incubated for 1–2 minutes in 1% Methylene blue solution Samples were examined in a Olympus SZ-III-Stereo Microscopes to see cell distribution on sample. Afterwards, samples underwent dehydration steps of 70–80–90–100%, 30 minutes per step. After dehydration, samples were critical point dried (CPD 030 Critical Point Dryer, Leica) and then gold sputtered at 40 mA and 100 mTorr for 30 seconds. The morphology of the cells was studied using a Philips XL30 ESEM-FEG SEM at 10 kV and a working distance of 10 mm.

Other fixated samples (n = 3), were permeabilized and block with TBP buffer (0.1% Triton X-100, 0.5% bovine serum albumin in PBS) overnight in 4°C. Cells were stained with Vinculin-FITC (1 : 400), Phalloidin-Texas Red (Molecular Probes, 1 : 100) and Dapi (1 : 100) with three times washing steps in between. Three images were taken for each sample, for a total of nine images by a fluorescence microscope (Nikon Eclipse E600) at magnification of 20× and 40×. Image analysis of vinculin was done by ImageJ to measure average area (A), perimeter (P), length, width, aspect ratio, circularity, density and sites per cell.

$$aspect = \frac{length}{width}$$

$$circularity = \frac{4\pi A}{p^2}$$

Average area is average area of vinculin sites of the cells attached, excluding the cells without vinculin expression. Vinculin density was calculated by including all the cells in the nine images and refers to the average area per area of cells, measured in percentage.

Enzyme-linked immunosorbent assay (ELISA) of TGF-β1, IL-1β, IL-6 and IL-10. Cell culture medium (n = 3) was collected at day 1, 4, and 7 before medium change. Cytokines secretion of TGF-β1, IL-1β, IL-6 and IL-10 was quantified using an ELISA assay according to the manufacturer's instructions (DuoSet ELISA development kit, R&D Systems Europe Ltd.).

Sircol and Fastin assay for collagen and elastin expression. Collagen samples (n = 6) at day 4 and 7, underwent collagen extraction using cold acid pepsin (0.1 mg/ml 0.5 M acetic acid) and left overnight in 4°C. Collagen isolation and concentration was done before adding the Sircol Dye Reagent. The assay was performed according to the picosirius red-based colorimetric SirCol™ collagen dye binding assay kit (Biocolor Ltd.) and measured at 540 nm. Rods (n = 6) for elastin quantification were firstly heated at 100°C for 1 hour period with oxalic acid (0.25 M) to extract α-elastin. Further elastin quantification was done following the Fastin elastin assay kit (Biocolor Ltd), measured at 513 nm.

Statistics analysis. All data are expressed as mean ± s.d. Biochemical assays were performed with triplicate biological sample, if not stated otherwise. Statistical analysis was done by Two-way Analysis of Variance (ANOVA) with Bonferroni's multiple comparison test ($p < 0.05$), unless otherwise indicated in the figure legends. For all figures the following applies: * = $p < 0.05$, ** = $p < 0.01$, *** = $p < 0.001$.

1. Anderson, J. M., Rodriguez, A. & Chang, D. T. Foreign body reaction to biomaterials. *Semin Immunol* **20**, 86–100 (2008).
2. Morais, J. M., Papadimitrakopoulos, F. & Burgess, D. J. Biomaterials/tissue interactions: possible solutions to overcome foreign body response. *Aaps j* **12**, 188–96 (2010).
3. Wang, Y., Papadimitrakopoulos, F. & Burgess, D. J. Polymeric "smart" coatings to prevent foreign body response to implantable biosensors. *Journal of Controlled Release* **169**, 341–347 (2013).
4. Boehler, R. M., Graham, J. G. & Shea, L. D. Tissue engineering tools for modulation of the immune response. *Biotechniques* **51**, 239–40, 242, 244 passim (2011).
5. Duffield, J. S., Lupher, M., Thannickal, V. J. & Wynn, T. A. Host Responses in Tissue Repair and Fibrosis. *Annual Review of Pathology: Mechanisms of Disease* **8**, 241–276 (2013).
6. Ko, I. K. *et al.* Combined systemic and local delivery of stem cell inducing/recruiting factors for in situ tissue regeneration. *Faseb j* **26**, 158–68 (2012).
7. Stevens, M. M. *et al.* In vivo engineering of organs: the bone bioreactor. *Proc Natl Acad Sci U S A* **102**, 11450–5 (2005).
8. Anderson, J. M. Biological responses to materials. *Annual Review of Materials Research* **31**, 81–110 (2001).
9. Papenburg, B. J., Rodrigues, E. D., Wessling, M. & Stamatialis, D. Insights into the role of material surface topography and wettability on cell-material interactions. *Soft Matter* **6**, 4377–4388 (2010).
10. Kumar, G., Waters, M. S., Farooque, T. M., Young, M. F. & Simon, C. G., Jr. Freeform fabricated scaffolds with roughened struts that enhance both stem cell proliferation and differentiation by controlling cell shape. *Biomaterials* **33**, 4022–30 (2012).
11. Shah, A., Shah, S., Mani, G., Wenke, J. & Agrawal, M. Endothelial cell behaviour on gas-plasma-treated PLA surfaces: the roles of surface chemistry and roughness. *J Tissue Eng Regen Med* **5**, 301–12 (2011).
12. Chen, S. *et al.* Characterization of topographical effects on macrophage behavior in a foreign body response model. *Biomaterials* **31**, 3479–91 (2010).
13. Holt, D. J., Chamberlain, L. M. & Grainger, D. W. Cell-cell signaling in co-cultures of macrophages and fibroblasts. *Biomaterials* **31**, 9382–94 (2010).
14. Pan, H., Jiang, H., Kantharia, S. & Chen, W. A fibroblast/macrophage co-culture model to evaluate the biocompatibility of an electrospun Dextran/PLGA scaffold and its potential to induce inflammatory responses. *Biomed Mater* **6**, 065002 (2011).
15. Zeng, Q. & Chen, W. The functional behavior of a macrophage/fibroblast co-culture model derived from normal and diabetic mice with a marine gelatin-oxidized alginate hydrogel. *Biomaterials* **31**, 5772–81 (2010).
16. Yamanami, M. *et al.* Implantation study of small-caliber "biotube" vascular grafts in a rat model. *J Artif Organs* **16**, 59–65 (2013).
17. Bakker, D., van Blitterswijk, C. A., Hesseling, S. C. & Grote, J. J. Effect of implantation site on phagocyte/polymer interaction and fibrous capsule formation. *Biomaterials* **9**, 14–23 (1988).

18. van Blitterswijk, C. A., van den Brink, J., Leenders, H. & Bakker, D. The effect of PEO ratio on degradation, calcification and bone bonding of PEO/PBT copolymer (PolyActive). **3**, 23–36 (1993).
19. van Dijkhuizen-Radersma, R. *et al.* Control of vitamin B12 release from poly(ethylene glycol)/poly(butylene terephthalate) multiblock copolymers. *Biomaterials* **23**, 1527–36 (2002).
20. France, R. M. & Short, R. D. Plasma treatment of polymers - Effects of energy transfer from an argon plasma on the surface chemistry of poly(styrene), low density poly(ethylene), poly(propylene) and poly(ethylene terephthalate). *Journal of the Chemical Society-Faraday Transactions* **93**, 3173–3178 (1997).
21. He, Q. G. *et al.* Preparation of hydrophilic poly(dimethylsiloxane) stamps by plasma-induced grafting. *Langmuir* **19**, 6982–6986 (2003).
22. Kim, K., Jeon, B.-J. & Jung, I. Preparation of CHF3 plasma polymeric composite membrane and characteristics of surface modification. *Korean Journal of Chemical Engineering* **17**, 33–40 (2000).
23. Gao, J., Niklason, L. & Langer, R. Surface hydrolysis of poly(glycolic acid) meshes increases the seeding density of vascular smooth muscle cells. *J Biomed Mater Res* **42**, 417–24 (1998).
24. Extrand, C. W. Criteria for ultralyophobic surfaces. *Langmuir* **20**, 5013–8 (2004).
25. Extrand, C. W. Contact angles and their hysteresis as a measure of liquid-solid adhesion. *Langmuir* **20**, 4017–21 (2004).
26. da Rocha-Azevedo, B. & Grinnell, F. Fibroblast morphogenesis on 3D collagen matrices: the balance between cell clustering and cell migration. *Exp Cell Res* **319**, 2440–6 (2013).
27. Yang, D., Lu, X., Hong, Y., Xi, T. & Zhang, D. The molecular mechanism of mediation of adsorbed serum proteins to endothelial cells adhesion and growth on biomaterials. *Biomaterials* **34**, 5747–58 (2013).
28. Berry, C. C., Campbell, G., Spadiccino, A., Robertson, M. & Curtis, A. S. The influence of microscale topography on fibroblast attachment and motility. *Biomaterials* **25**, 5781–8 (2004).
29. Lee, J. H., Lee, S. J., Khang, G. & Lee, H. B. Interaction of fibroblasts on polycarbonate membrane surfaces with different micropore sizes and hydrophilicity. *J Biomater Sci Polym Ed* **10**, 283–94 (1999).
30. Novak, M. L. & Koh, T. J. Macrophage phenotypes during tissue repair. *J Leukoc Biol* **93**, 875–81 (2013).
31. Sica, A. & Mantovani, A. Macrophage plasticity and polarization: in vivo veritas. *J Clin Invest* **122**, 787–95 (2012).
32. Hao, N. B. *et al.* Macrophages in tumor microenvironments and the progression of tumors. *Clin Dev Immunol* **2012**, 948098 (2012).
33. Taylor, A. W. Review of the activation of TGF-β in immunity. *Journal of Leukocyte Biology* **85**, 29–33 (2009).
34. Rihova, B. Biocompatibility of biomaterials: hemocompatibility, immunocompatibility and biocompatibility of solid polymeric materials and soluble targetable polymeric carriers. *Advanced Drug Delivery Reviews* **21**, 157–176 (1996).
35. DeFife, K. M., Colton, E., Nakayama, Y., Matsuda, T. & Anderson, J. M. Spatial regulation and surface chemistry control of monocyte/macrophage adhesion and foreign body giant cell formation by photochemically micropatterned surfaces. *J Biomed Mater Res* **45**, 148–54 (1999).
36. Tamada, Y. & Ikada, Y. Fibroblast growth on polymer surfaces and biosynthesis of collagen. *J Biomed Mater Res* **28**, 783–9 (1994).
37. Kim, K. *et al.* The influence of stereolithographic scaffold architecture and composition on osteogenic signal expression with rat bone marrow stromal cells. *Biomaterials* **32**, 3750–63 (2011).
38. Barth, K. A., Waterfield, J. D. & Brunette, D. M. The effect of surface roughness on RAW 264.7 macrophage phenotype. *J Biomed Mater Res A* **101**, 2679–88 (2013).
39. Schwartz, Z. *et al.* Effect of micrometer-scale roughness of the surface of Ti6Al4V pedicle screws in vitro and in vivo. *J Bone Joint Surg Am* **90**, 2485–98 (2008).
40. Odelius, K. *et al.* Porosity and pore size regulate the degradation product profile of polylactide. *Biomacromolecules* **12**, 1250–8 (2011).
41. Walter, R., Kannan, M. B., He, Y. & Sandham, A. Effect of surface roughness on the in vitro degradation behaviour of a biodegradable magnesium-based alloy. *Applied Surface Science* **279**, 343–348 (2013).
42. Linker-Israeli, M. *et al.* Exogenous IL-10 and IL-4 down-regulate IL-6 production by SLE-derived PBMC. *Clinical Immunology* **91**, 6–16 (1999).
43. Marie, C., Pitton, C., Fitting, C. & Cavaillon, J. M. Regulation by anti-inflammatory cytokines (IL-4, IL-10, IL-13, TGF beta) of interleukin-8 production by LPS- and/or TNF alpha-activated human polymorphonuclear cells. *Mediators of Inflammation* **5**, 334–340 (1996).
44. Hamlet, S., Alfarsi, M., George, R. & Ivanovski, S. The effect of hydrophilic titanium surface modification on macrophage inflammatory cytokine gene expression. *Clin Oral Implants Res* **23**, 584–90 (2012).
45. Babensee, J. E. Interaction of dendritic cells with biomaterials. *Semin Immunol* **20**, 101–8 (2008).
46. Seong, S. Y. & Matzinger, P. Hydrophobicity: an ancient damage-associated molecular pattern that initiates innate immune responses. *Nat Rev Immunol* **4**, 469–78 (2004).
47. Moyano, D. F. *et al.* Nanoparticle Hydrophobicity Dictates Immune Response. *Journal of the American Chemical Society* **134**, 3965–3967 (2012).
48. Hoelzle, M. K. & Svitkina, T. The cytoskeletal mechanisms of cell–cell junction formation in endothelial cells. *Molecular Biology of the Cell* **23**, 310–323 (2012).
49. Kolacna, L. *et al.* Biochemical and biophysical aspects of collagen nanostructure in the extracellular matrix. *Physiol Res* **56 Suppl 1**, S51–60 (2007).
50. Karnik, S. K. *et al.* A critical role for elastin signaling in vascular morphogenesis and disease. *Development* **130**, 411–23 (2003).
51. Brooke, B. S., Bayes-Genis, A. & Li, D. Y. New insights into elastin and vascular disease. *Trends Cardiovasc Med* **13**, 176–81 (2003).
52. Patel, A., Fine, B., Sandig, M. & Mequanint, K. Elastin biosynthesis: The missing link in tissue-engineered blood vessels. *Cardiovasc Res* **71**, 40–9 (2006).
53. Wognum, S., Schmidt, D. E. & Sacks, M. S. On the mechanical role of de novo synthesized elastin in the urinary bladder wall. *J Biomech Eng* **131**, 101018 (2009).
54. Kenyon, N. J., Ward, R. W., McGrew, G. & Last, J. A. TGF-beta1 causes airway fibrosis and increased collagen I and III mRNA in mice. *Thorax* **58**, 772–7 (2003).
55. Horstmeyer, A., Licht, C., Scherr, G., Eckes, B. & Krieg, T. Signalling and regulation of collagen I synthesis by ET-1 and TGF-beta1. *Febs j* **272**, 6297–309 (2005).
56. Baranek, T. *et al.* Elastin receptor (Spliced galactosidase) occupancy by elastin peptides counteracts proinflammatory cytokine expression in lipopolysaccharide-stimulated NF-kappa B down-regulation. *Journal of Immunology* **179**, 6184–6192 (2007).
57. Petrella, B. L., Armstrong, D. A. & Vincenti, M. P. Interleukin-1 beta and transforming growth factor-beta 3 cooperate to activate matrix metalloproteinase expression and invasiveness in A549 lung adenocarcinoma cells. *Cancer Lett* **325**, 220–6 (2012).
58. John, T. *et al.* Effect of pro-inflammatory and immunoregulatory cytokines on human tenocytes. *J Orthop Res* **28**, 1071–7 (2010).
59. Hong, H. H. & Trackman, P. C. Cytokine regulation of gingival fibroblast lysyl oxidase, collagen, and elastin. *J Periodontol* **73**, 145–52 (2002).
60. Moroni, L. & Lee, L. P. Micropatterned hot-embossed polymeric surfaces influence cell proliferation and alignment. *J Biomed Mater Res A* **88**, 644–53 (2009).

Acknowledgments

This research forms part of the Project P3.03 DialysisXS of the research program of the BioMedical Materials institute, co-funded by the Dutch Ministry of Economic Affairs, Agriculture and Innovation. The financial contribution of the Nierstichting Nederland is gratefully acknowledged. Contribution of PCL rods provided from Xeltis, the Netherlands is gratefully appreciated.

Author contributions

F.F.R.D., L.M., T.C.R., C.V. and J.I.R. were involved in the design of the experiments. F.F.R.D. conducted experiments and analysed data. F.F.R.D. and L.M. wrote the manuscript. J.I.R. and L.M. initiated the project. All authors discussed the results and commented on the paper.

Additional information

Supplementary information accompanies this paper at http://www.nature.com/scientificreports

Competing financial interests: The authors declare no competing financial interests.

How to cite this article: Damanik, F.F.R., Rothuizen, T.C., van Blitterswijk, C., Rotmans, J.I. & Moroni, L. Towards an in vitro model mimicking the foreign body response: tailoring the surface properties of biomaterials to modulate extracellular matrix. *Sci. Rep.* **4**, 6325; DOI:10.1038/srep06325 (2014).